Korean J. Chem. Eng., 39(8), 2172-2181 (2022)
DOI: 10.1007/s11814-021-1039-2

pISSN: 0256-1115
eISSN: 1975-7220

Preparation of gold decorated MoS_2/NiO nanocomposite in the production of a new electrochemical sensor for ascorbic acid detection

Keziban Atacan*,,***,†, Nuray Güy***,****, and Mahmut Özacar***,****

*Sakarya University, Biomedical, Magnetic and Semiconductor Materials Application and Research Center (BIMAS-RC), 54187 Sakarya, Turkey
**Sakarya University of Applied Sciences, Akyazı Vocational School of Health Services, 54400 Sakarya, Turkey
***Sakarya University, Biomaterials, Energy, Photocatalysis, Enzyme Technology, Nano & Advanced Materials, Additive Manufacturing, Environmental Applications and Sustainability Research & Development Group (BIOENAMS R & D Group), 54187 Sakarya, Turkey
****Sakarya University, Science & Arts Faculty, Department of Chemistry, 54187 Sakarya, Turkey
(*Received 26 October 2021 • Revised 4 December 2021 • Accepted 13 December 2021*)

Abstract−We investigated electrochemical sensing of ascorbic acid by Au-MoS_2/NiO modified glassy carbon electrode. The MoS_2, NiO, MoS_2/NiO were prepared by hydrothermal , and Au-MoS_2/NiO was prepared chemical reduction method. The characterization of Au-MoS_2/NiO composite was carried out using X-ray diffraction, Fourier transform infrared spectroscopy, X-ray photoelectron spectroscopy and field emission scanning electron microscopy. The electrochemical characteristics of the Au-MoS_2/NiO composite were examined by cyclic voltammetry and electrochemical impedance spectroscopy. Then, differential pulse voltammetry responses of Au-MoS_2/NiO modified glassy carbon electrode were detected towards the ascorbic acid in phosphate buffer (0.1 M, pH=7). The ascorbic acid sensor represented low detection limit of 0.13 μM with linear range of 2-50 μM, revealing that this sensor gave satisfactory responses. The practical feasibility of the obtained sensor was assessed for the detection of ascorbic acid in Vitamin C tablet. We believe that this study could help different studies for producing commercially ascorbic acid sensors.

Keywords: NiO, MoS_2, Electrochemical Sensor, Low Detection Limit, Ascorbic Acid

INTRODUCTION

Ascorbic acid (AA) is a prominent water-soluble vitamin and vital ingredient in individual nutrition [1,2]. However, an abnormal level of AA is usually a symptom of an illness, such as mental and scurvy. So the improvement of sensitive and selective detection techniques for its biological investigation is significant [1,2]. The usual ingredients of AA in the human body should maintain at 70-90 mg [3]. The toxicity of AA is very rare, and more than 2,000 mg/day is not advised as it can cause stomach upset and diarrhea [4]. For this reason, it is of great relevance to evolve proper and influential ways to detect AA in medicine and food [5]. So far, many different methods, such as capillary electrophoresis [6], gas chromatography [7], colorimetry [8,9] and chemiluminescence [10], have been stated for the determination of AA in scientific studies carried out. But, these techniques have disadvantages such as high cost, operational complexity and laborious sample treatments [4]. In recent years, electrochemical methods have been considered in the determination of AA due to its benefits, such as good selectivity, rapid response, high sensitivity, and low cost [2,11]. Although AA is an electroactive material, its use alone is difficult because of direct detection using traditional electrodes such as glassy carbon, graphite, and platinum due to fouling of the electrode and poor selectivity [12]. To prevent these, studies are of interest using nanomaterials modified electrodes for AA detection.

Molybdenum disulfide (MoS_2) has been commonly investigated owing to its superb optical and electrochemical features [11,13]. MoS_2 has a similar structure to graphene and can be considered a semiconductor, which can be effectively combined with metal nanoparticles [14]. Moreover, MoS_2 has been recognized as a supporting material used to stabilize metal nanoparticles and create specially designed structures [15]. Murugan et al. improved a flower-structured molybdenum disulfide (MoS_2)-decorated functionalized multiwall carbon nanotube (f-MWCNTs)/zinc oxide (ZnO) for detection of AA [11].

Transition metal nanoparticles, metal oxides, and alloy nanoparticles have become the most preferred nanomaterials in bio-sensing studies [1]. Nickel oxide (NiO) is a transition metal oxide with interesting electronic, low toxicity, optical, electrochemical, and electro-catalytic features [16]. NiO has a large surface-to-volume ratio and reversible electrochemical reaction, suggesting it is suitable for use as electrode material in electrochemistry [17]. Swamy and coworkers studied NiO/graphene modified graphite electrodes for the detection of dopamine (DA), tyrosine (Tyr), and AA [18].

Noble metal-based nanoparticles (NPs), such as gold (Au), platinum (Pt), and silver (Ag), are quite glamorous nanomaterials due to pore size, large volume to the surface area, good conductivity, and great electro-catalytic activity [1,19]. The composite conduction of

†To whom correspondence should be addressed.
E-mail: kezibanatacan@sakarya.edu.tr

Au, Pt, and Ag on electrodes has been evidenced as an influential way to decrease the charge transfer resistance and accelerate electron conduction [1,19]. Ngo et al. reported that a non-enzymatic glucose sensor is fabricated using Ag/NiO/rGO nanostructure [20]. So, they proved that Ag nanoparticles could boost the electrocatalytic efficiency by increasing electron-hole separation throughout the electro-oxidation/reduction processes [20]. Chen and colleagues improved the MoS_2/Au nanocomposites for electrochemical detection of dopamine [21]. They preferred Au nanoparticles because of their large surface area or high catalytic activity [21]. Au was preferred to increase the conductivity of metal oxide semiconductor nanocomposite in this study with this in mind.

In this work, we advanced a new electrochemical sensor for the desirable detection of AA utilizing gold nanoparticle-decorated MoS_2/NiO. We doped with Au metal on MoS_2/NiO because of increasing the active surface area and improving the electronic properties of the composite, which may lead to a higher sensor response than that of pure nanostructures. First, a novel Au-MoS_2/NiO composite was prepared and dropped onto a glassy carbon electrode (GCE) surface and then evaluated to detect AA. So, the advantage of the Au-MoS_2/NiO/GCE sensor is the precise control of AA for determining conspicuous reproductivity and excellent stability.

EXPERIMENTAL

The details of chemicals and apparatus are contained within Supplementary Material.

1. Synthesis of Au-MoS_2/NiO Composite

First, MoS_2 was prepared using a hydrothermal method reported by Yu et al. [22]. 2.2 g of $(NH_4)_6Mo_7O_{24}$ and 2.0 g of thiourea were dissolved in 80 mL of distilled water (DW) under ultrasonication for 30 min. After that, the mixture was taken into a Teflon-lined autoclave and maintained at 200 °C for 16 h in the oven. Finally, the obtained black precipitate was washed with water and ethanol, centrifuged, and dried at 60 °C for overnight.

For the fabrication of MoS_2/NiO, 0.06 g of MoS_2 was dispersed in deionized water (DW, 20 mL) under ultrasonication for 15 min. Then, 0.12 g of $NiCl_2{\cdot}6H_2O$ was dissolved in DW under sonication. The mixture was transferred into a Teflon-lined stainless steel autoclave and kept at 120 °C for 2 h [14]. Finally, the MoS_2/NiO composite was washed with DW and ethanol, respectively, and dried at 60 °C for overnight. For comparison, the preparation of the pure

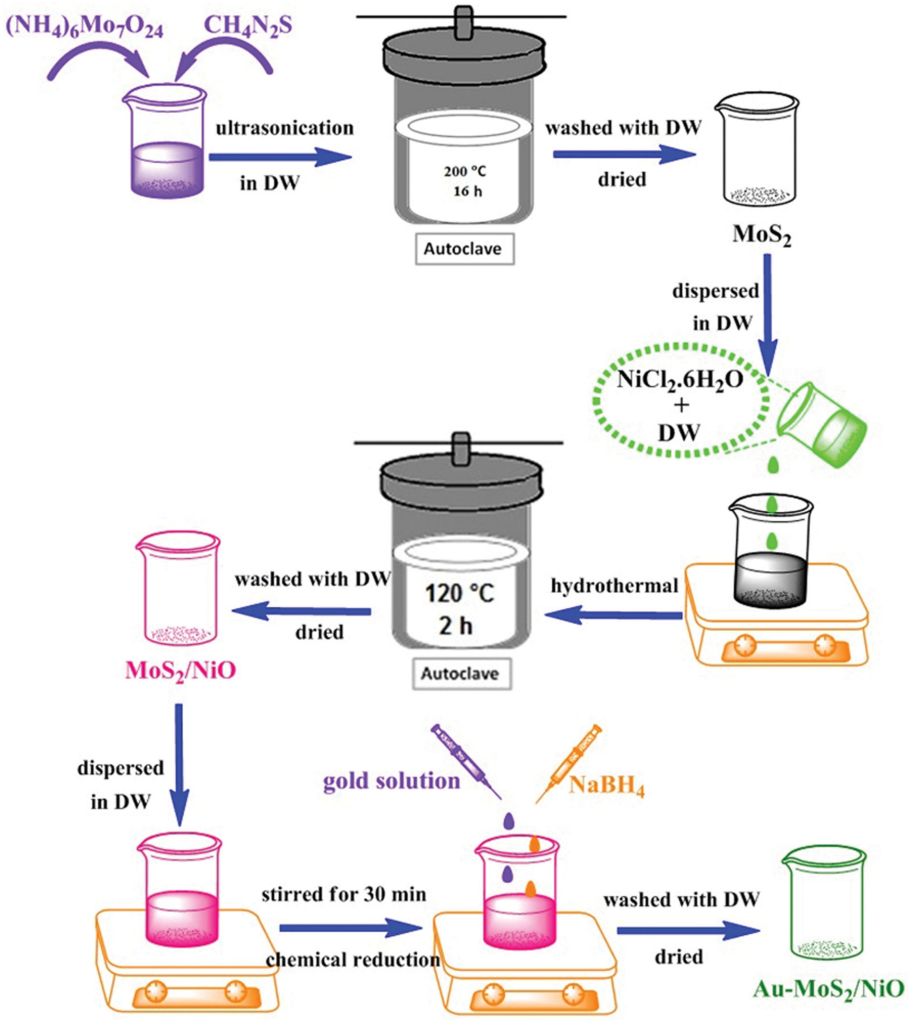

Scheme 1. Schematic pathways of preparing Au-MoS_2/NiO composite.

NiO was carried out using the same above method without using MoS_2.

To prepare Au-MoS_2/NiO composite, the authors used the chemical reduction method reported by the Atacan study [23]. 50 mg of MoS_2/NiO composite was suspended in 20 mL of DW utilizing a sonicator for 15 min. Next, 1,250 µL of the gold standard solution was added into the dispersion and stirred for 30 minutes. 1,250 µL of $NaBH_4$ (0.2 M) as a reduction agent was added into the mixture. The solution of Au-MoS_2/NiO was centrifuged and washed with, dried at 60 °C. The preparation of Au-MoS_2/NiO composite is illustrated in Scheme 1.

2. Preparation of the Au-MoS_2/NiO Modified GCE

GCE (with a geometrical area of 0.071 cm^2) was polished with 0.3 µm α-alumina powder and sonicated with DW and ethanol, respectively. Au-MoS_2/NiO (3 mg mL^{-1}) containing 0.5% Nafion was dispersed under ultrasonication for 10 min. Au-MoS_2/NiO

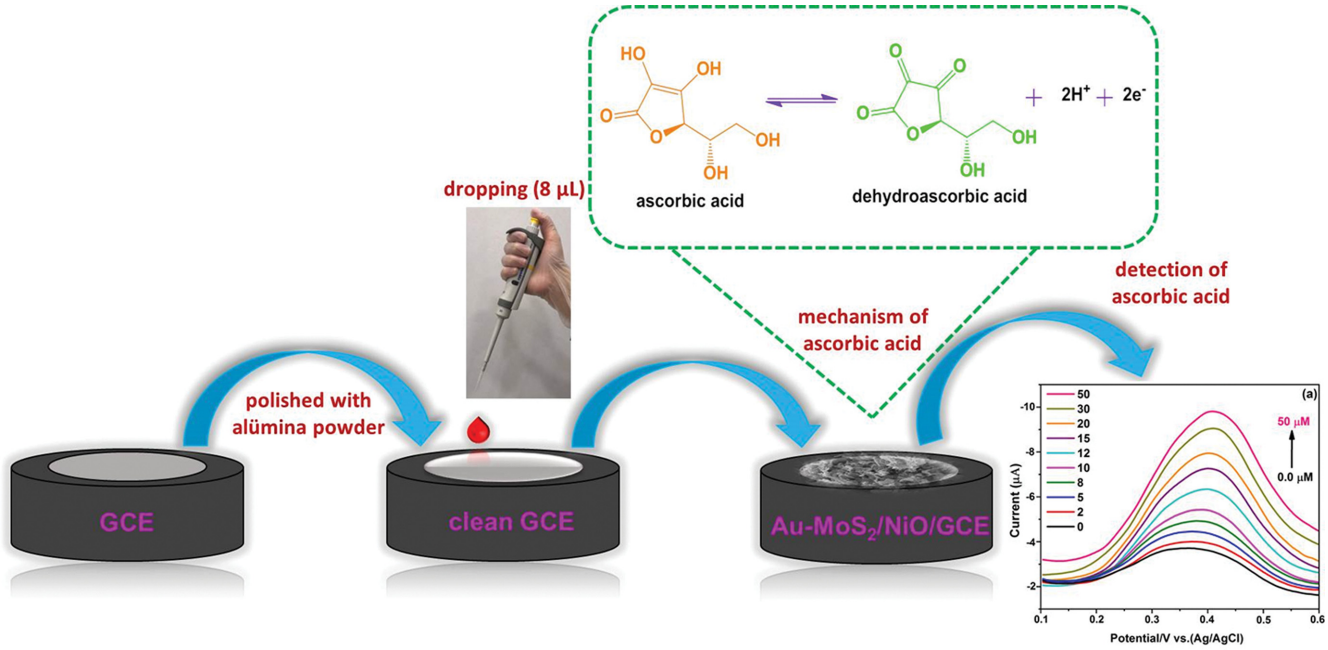

Scheme 2. The fabrication of Au-MoS_2/NiO composite on GCE for AA detection.

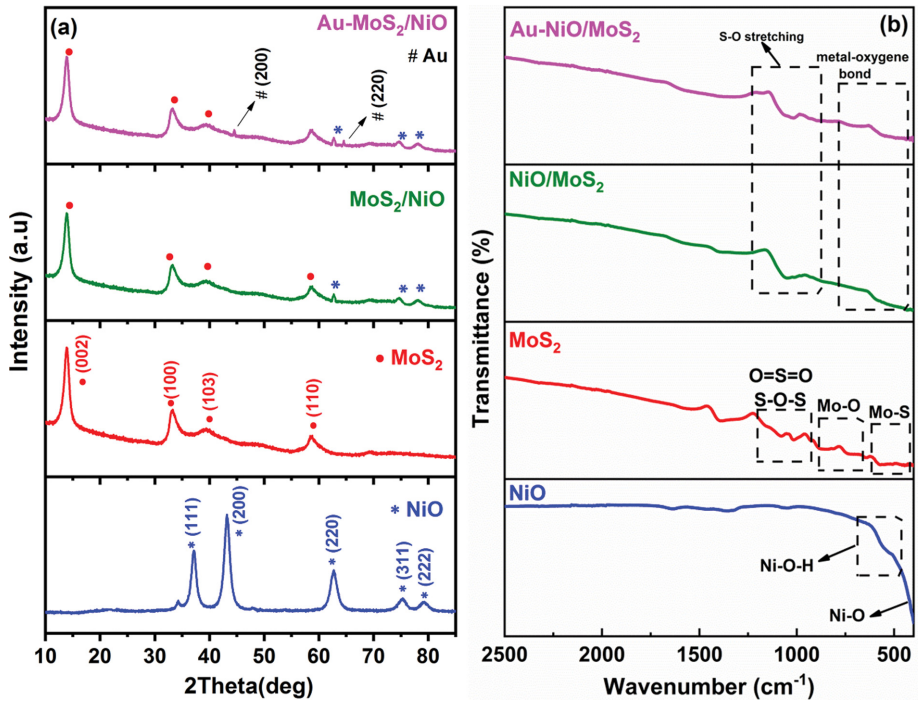

Fig. 1. XRD patterns (a) and FTIR spectra (b) of all samples.

(8 μL) was dropped on the clean GCE and dried at room temperature. Different volumes of the nanocomposite were dropped on GCE such as 3, 5, 8, 10 μL (Supplementary Material, Fig. S1). The optimal volume of Au-MoS_2/NiO nanocomposite coating on the surface of GCE was found to be 8 μL. This result may be due to the excessive increase in the amount of Au-MoS_2/NiO on the electrode surface, negatively affecting the electron transfer process between the sensor and the analyte [24]. The process of fabrication of Au-MoS_2/NiO on GCE is delineated in Scheme 2. In addition, the modified electrode was denoted as Au-MoS_2/NiO/GCE. Similarly, MoS_2/GCE, NiO/GCE, and MoS_2/NiO/GCE were fabricated in the aforementioned method. All experiments were concluded by measuring three times. The data were represented as the averaged value (standard deviation is ±3%).

RESULTS AND DISCUSSION

1. Characterization of Samples

The crystal structure of samples was also analyzed by XRD (Fig. 1(a)). The XRD pattern of NiO depicts peaks at 37.1°, 43.3°, 62.7°, 75.2°, 79.4°, which correspond to (111), (200), (220), (222) and (311) the crystal planes, respectively (JCPDS no. 04-0835) [25-27]. For MoS_2, the observed peaks at 14.1°, 33.2°, 39.4°, and 58.6° are indexed to (002), (100), (103) and (110) planes of the single-phase MoS_2 (JCPDS no. 37-1492) [14]. For MoS_2/NiO, the diffraction peaks represented in Fig. 1(a) evidence the presence of both NiO and MoS_2 in the nanocomposite. The XRD pattern of Au-MoS_2/NiO is similar to that of MoS_2/NiO, but there are also Au peaks observed at 44.5° and 64.5° corresponding to the planes (200) and

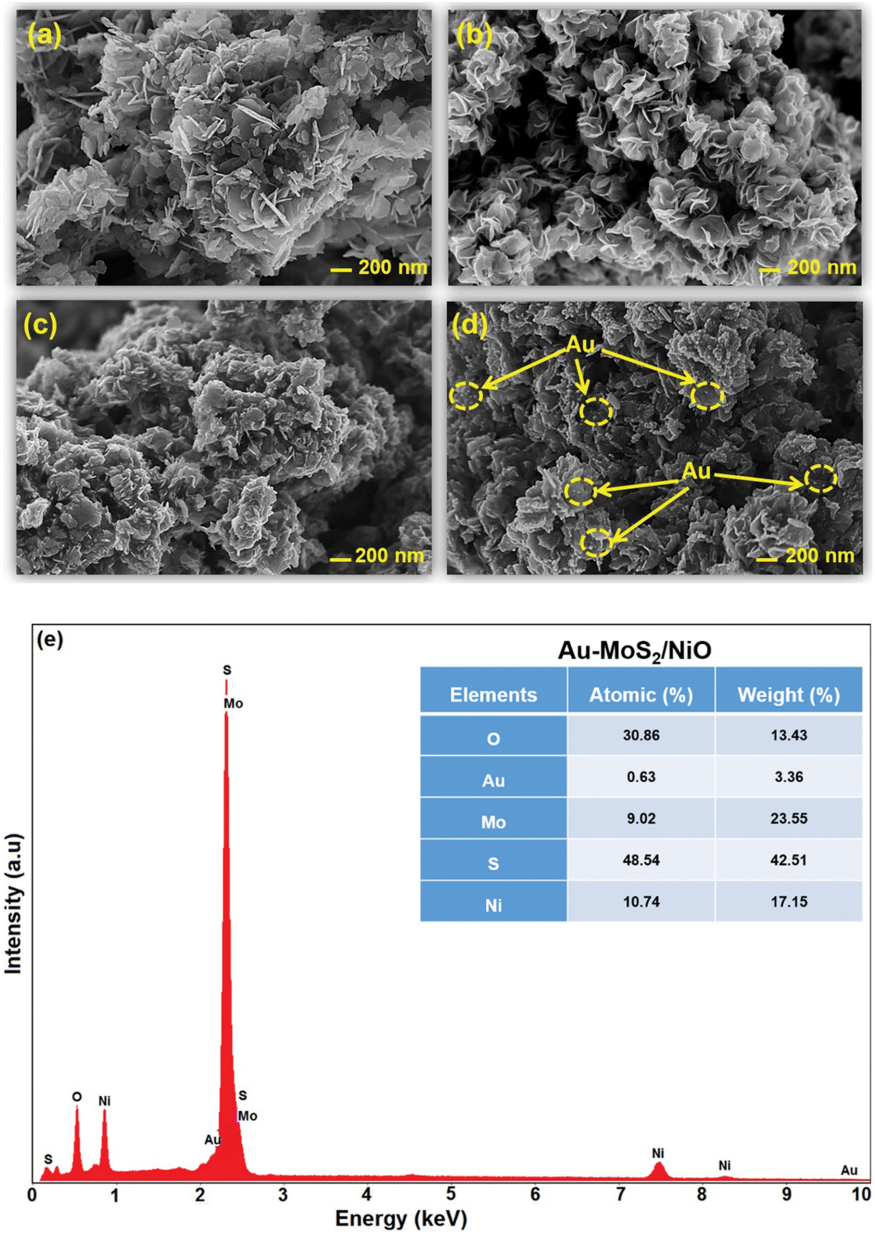

Fig. 2. SEM photographs of NiO (a), MoS_2 (b), MoS_2/NiO (c), Au-MoS_2/NiO (d) and EDX spectrum (e) of Au-MoS_2/NiO.

(220) in the XRD pattern of Au-MoS_2/NiO [28,29]. The detected diffraction peaks of NiO, MoS_2, and Au in the Au-MoS_2/NiO nanocomposite prove that the Au-MoS_2/NiO has been successfully prepared in Fig. 1(a).

Fig. 1(b) demonstrates the FTIR spectra of the synthesized products. The FTIR spectrum of NiO indicates a strong band at 429 cm^{-1} corresponding to the vibration of the Ni-O bond [30-32], but the absorption bond between 497 and 677 cm^{-1} is associated to Ni-O-H stretching bond [30,32]. The peak at about 564 cm^{-1} for MoS_2 was assigned to Mo-S vibration [33]. The peaks between 730 cm^{-1} and 900 cm^{-1} are attributable to the stretching vibrations of Mo-O. Also, the peaks at 1,115 cm^{-1} and 1,030 cm^{-1} correspond to the bending vibrations of O=S=O and S-O-S, respectively [34]. In the case of the MoS_2/NiO and Au-MoS_2/NiO, the prominent peak at 1,043 cm^{-1} belongs to S-O stretching, and a peak at about 600 cm^{-1} confirms the presence of metal-oxygen bond in these composites. The characteristic peaks of the Au-MoS_2/NiO composites are consistent with that of MoS_2/NiO.

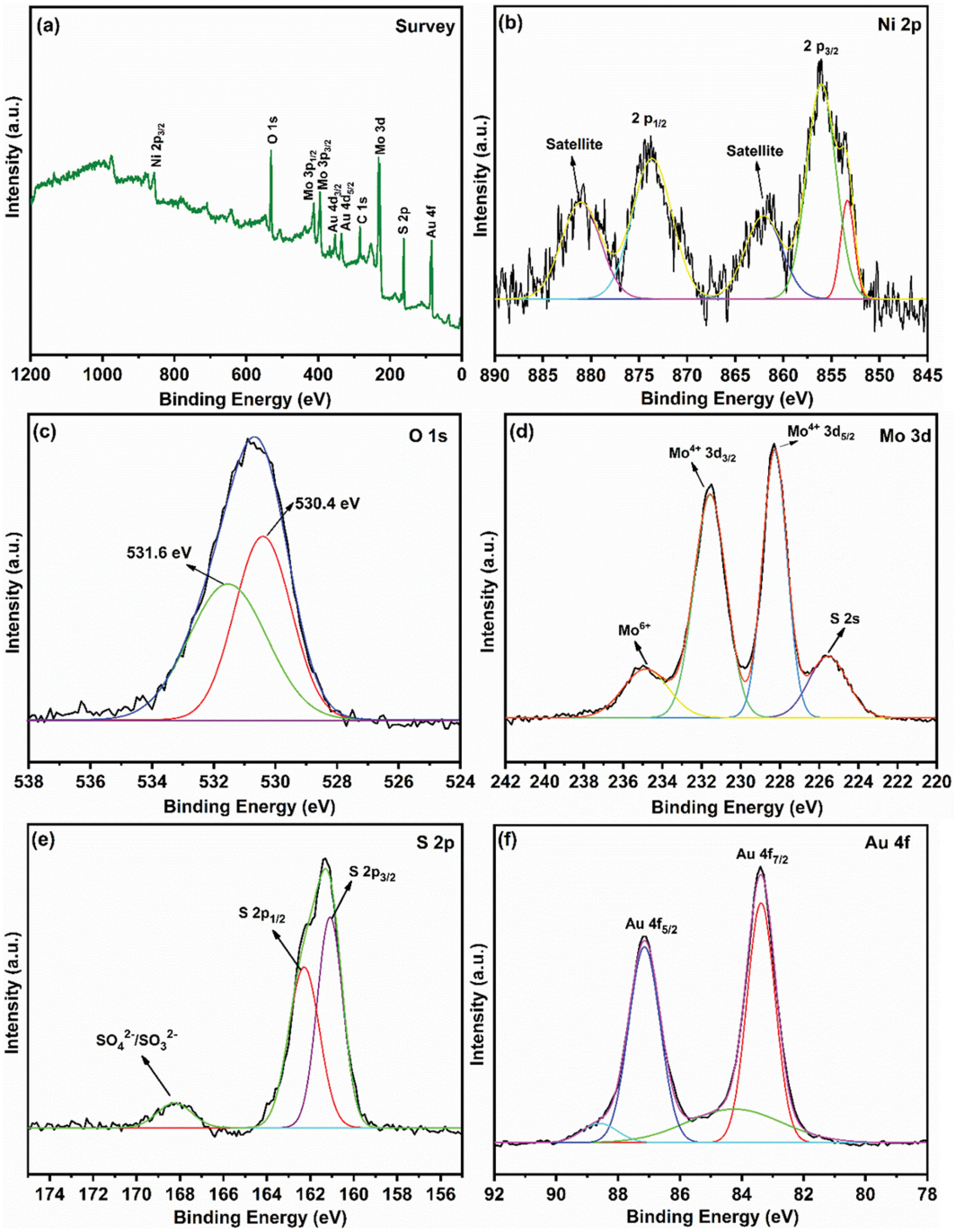

Fig. 3. XPS spectra of Au-MoS_2/NiO nanocomposite (a) XPS survey spectrum, (b) Ni 2p spectrum, (c) O 1s spectrum, (d) Mo 3d spectrum, (e) S 2s spectrum and (f) Au 3f spectrum.

Fig. 2 depicts the SEM photos of NiO (a), MoS_2 (b), MoS_2/NiO (c) and Au-MoS_2/NiO (d). As shown in Fig. 2(a), NiO exhibits the structure of flake and wrinkle morphology. The image of MoS_2 illustrates the nanosheet-like structure in Fig. 2(b). Fig. 2(c) shows the SEM image of MoS_2/NiO, both MoS_2/NiO in which NiO nanoparticles are incorporated into the nanocomposite and also shows that MoS_2/NiO has a wrinkled structure, possibly caused by hydrothermal processing [14,35,36]. Au nanoparticles are doped only to a minor extent on MoS_2/NiO binary nanocomposite in Fig. 2(d). EDX was carried out showing the elemental composition of Au-MoS_2/NiO (Fig. 2(e)), which verified the presence of Ni, O, Mo, S, and Au without any other impurities. Also, the weight and atomic percentages of all elements were described at the table of elemental compositions of Au-MoS_2/NiO in Fig. 2(e) inset. Thus, the results prove the formation of the Au-MoS_2/NiO nanocomposite.

The surface element composition and chemical state of the Au-MoS_2/NiO nanocomposite were studied by X-ray photoelectron spectroscopy (XPS). As represented in Fig. 3(a), the XPS survey spectrum supplies the existence of Ni, O, Mo, S, and Au elements in the nanocomposite. In Fig. 3(b), two main peaks at 855.9 eV and 873.8 eV were attributed to Ni $2p_{3/2}$ and Ni $2p_{1/2}$, respectively, and their corresponding satellite/shoulder peaks were observed at 862.1 eV and 881.1 eV [37]. The observed two peaks at 530.4 eV and 531.6 eV can be assigned to the lattice oxygen of NiO and the adsorbed hydroxyl group on the surface of NiO, respectively in Fig. 3(c) [38]. Fig. 3(d) specifies the XPS spectrum of Mo 3d. The peaks at 228.4 eV (Mo $3d_{5/2}$) and 231.6 eV (Mo $3d_{3/2}$) correspond to the Mo(IV), while the peak at 236.1 eV is ascribed to Mo(VI), owing to partial oxidation of Mo(IV). Additionally, the peak at 225.6 eV depicts S^{2-} ions [38]. S 2p spectrum (Fig. 3(e)) depicts that two peaks at 161.1 and 162.4 eV correspond to S $2p_{3/2}$ in MoS_2, respectively [39]. The peak at 168.2 corresponds to SO_4^{2-}/SO_3^{2-}, which is formed by the oxidation of sulfur throughout the hydrothermal process [39]. From Fig. 3(f), it can be observed that the Au 4f region indicates obvious peaks at 87.14 and 83.4 eV, ascribed to $4f_{5/2}$ and $4f_{7/2}$ of Au^0. Furthermore, two peaks at 88.6 and 84.3 eV could be assigned to $4f_{5/2}$ and $4f_{7/2}$ of Au^+, respectively [40]. The XPS analysis reveals that Au-MoS_2/NiO nanocomposite has been successfully produced in this process.

2. Electrochemical Measurements of All Modified GCEs

Electrochemical impedance spectroscopy (EIS) is a strong technique for the electrode modification process. The Nyquist plots for GCE, NiO/GCE, MoS_2/GCE, MoS_2/NiO/GCE, Au-MoS_2/NiO/GCE, and the equivalent circuit utilized to comply with the acquired EIS

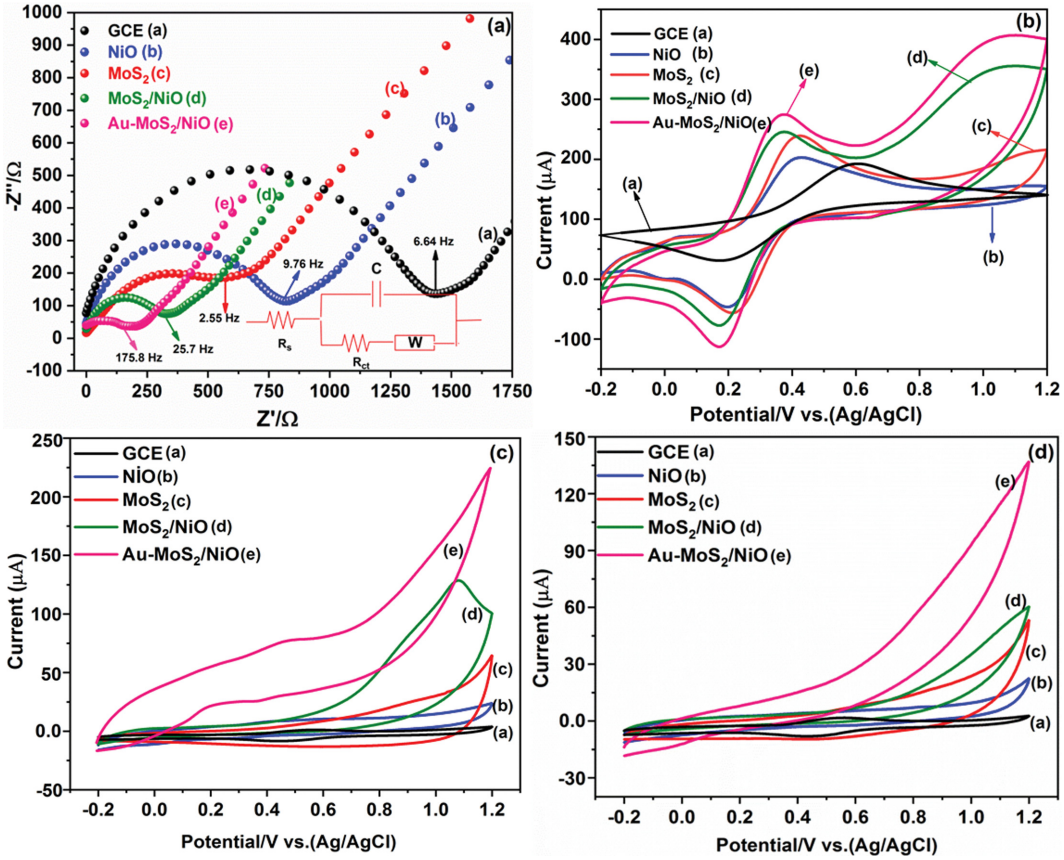

Fig. 4. (a) Nyquist diagrams of EIS in 0.1 M KCl containing $K_{3/4}Fe(CN)_6$ for GCE and all modified GCE (AC frequency range: 0.01 Hz to 1,000 Hz; AC amplitude: 5.0 mV). Inset: The Randles equivalent circuit model, where the parameters such as R_s, R_{ct}, C and W symbolize the solution resistance, the electron transfer resistance, the constant phase element corresponding to the double-layer capacitance and the Warburg constant, respectively, (b) CV curves in 0.1 M KCl containing $K_{3/4}Fe(CN)_6$ at scan rate 50 mV s^{-1} for GCE and all modified GCE, (c) CV curves in the presence of 1 mM AA in 0.1 M phosphate buffer (pH=7) at scan rate 50 mV s^{-1} and (d) CV curves in the absence of AA in 0.1 M phosphate buffer (pH=7) at scan rate 50 mV s^{-1} for GCE and all modified GCE.

result are displayed in Fig. 4(a) and Fig. 4(a) inset, respectively. The experiments were performed in 0.1-1,000 Hz frequency range and at 0.005 V amplitude. The semicircle diameter found in Nyquist plots is equal to the electron transfer resistance (Rct), checking the electron transfer properties of the redox probe on the electrode surface [41]. From Nyquist plots from the diameter of the semicircles, it was found that the Au-MoS_2/NiO/GCE (152 Ω) has a low Rct compared to GCE (1,420 Ω), NiO/GCE (805 Ω), MoS_2/GCE (580 Ω) and MoS_2/NiO/GCE (329 Ω). Rct was found that it is lower because Au nanoparticles have both good conductivity and a large surface area on the GCE surface [16]. The EIS results confirmed that the conductivity of the nanocomposite was boosted owing to available affirmative interactions between Au-MoS_2/NiO/GCE and the electrolyte.

Fig. 4(b) indicates CV curves of GCE, NiO/GCE, MoS_2/GCE, MoS_2/NiO/GCE, and Au-MoS_2/NiO/GCE in 0.1 M KCl containing $[Fe(CN)_6]^{3-/4-}$ at scan rate 50 mV s^{-1}. As illustrated in Fig. 4(b), Au-MoS_2/NiO/GCE indicates the largest peak current values, indicating greater conductivity than GCE, NiO/GCE, MoS_2/GCE and MoS_2/NiO/GCE. Well-defined redox peaks for $[Fe(CN)_6]^{3-/4-}$, the couple is clearly observed on all the modified electrodes. The lowest redox peak is sighted on the CV curve of NiO/GCE, depicting weaker conductivity than the other modified electrodes. Moreover, the electrochemical surface areas of all modified electrodes were calculated using Randles-Sevcik equation (Eq. (1)) [24,42].

$$I_p=(2.69\times10^5)n^{3/2}AC^*D^{1/2}v^{1/2} \quad (1)$$

where I_p represents the redox peak current (μA); n is the number of electrons transferred in the redox reaction; D belongs to the diffusion coefficient in solution ($K_{3/4}Fe(CN)_6$=7.6×10^{-6} cm^2 s^{-1}); A is the effective surface area of the electrode in cm^2; C^* is the concentration of $K_{3/4}Fe(CN)_6$ in mol cm^{-3} which is 0.1; v is the scan rate (50 mV s^{-1}). The effective surface areas of modified electrodes were calculated from the slope of the I_p versus $\upsilon^{1/2}$ plot. The electroactive surface area of Au-MoS_2/NiO/GCE was computed as 0.3518 cm^2 in comparison with GCE (0.071 cm^2), indicating the highest value than the other modified electrodes. After Au nanoparticles were modified, the anodic and cathodic currents were stronger than before, owing to the relatively poor conductivity of NiO or MoS_2 [43]. The electroactive surface areas of MoS_2/NiO/GCE, MoS_2/GCE, and NiO/GCE were estimated to be 0.2905 cm^2, 0.2840 cm^2, and 0.2646 cm^2, respectively. This result can be estimated as high dispersion of NiO nanoparticles on MoS_2 nanosheets increasing the active sites [43]. These results indicate that Au-MoS_2/NiO/GCE has an extensive surface area on the bare GCE surface [44]. It is compatible with, and further verifies, the result found from EIS tests.

Fig. 4(c) represents the CVs of GCE, NiO/GCE, MoS_2/GCE, MoS_2/NiO/GCE, and Au-MoS_2/NiO/GCE in 0.1 M phosphate buffer (pH=7) in the existence of 1 mM AA. Compared to the other modified GCE, Au-MoS_2/NiO/GCE exhibited the highest peak current, which represented Au's contribution because of its superb electrical conductivity, large surface area, and more electroactive interaction sites [16,44]. Fig. 4(d) depicts the CVs of GCE, NiO/GCE, MoS_2/GCE, MoS_2/NiO/GCE, and Au-MoS_2/NiO/GCE in 0.1 M phosphate buffer (pH=7) in the absence of AA. Au-MoS_2/NiO/GCE had the highest current, but no oxidation peak was sighted due to the absence of AA. If we look at the data in both the presence and absence of AA, the results demonstrate that the Au-MoS_2/NiO/GCE possesses a high current for the detection of AA compared with the other modified GCEs.

For electrochemical behavior, the scan rate and pH effect of AA on Au-MoS_2/NiO/GCE were studied in the range from −0.2 V to 1.2 V using the CV method. The scan rate effect of the Au-MoS_2/NiO/GCE toward the oxidation of 1 mM AA in 0.1 M phosphate buffer (pH=7) was analyzed at the variation of scan rates (20.0-300.0 mV s^{-1}) in Fig. 5(a). The plot of anodic peak currents against square root of scan rates ($\upsilon^{1/2}$) is depicted in Fig. 5(a) inset. The results indicate that the peak current increased with increasing scan rate. This result indicates that the oxidation of AA is a diffusion-controlled electrochemical process on the Au-MoS_2/NiO/GCE [11,45]. The fitting equation was calculated as $I_{(pa)}$=1.3541×$\upsilon^{1/2}$−6.9641 (R^2=0.9981). Fig. 5(b) displays the evaluation of Au-MoS_2/

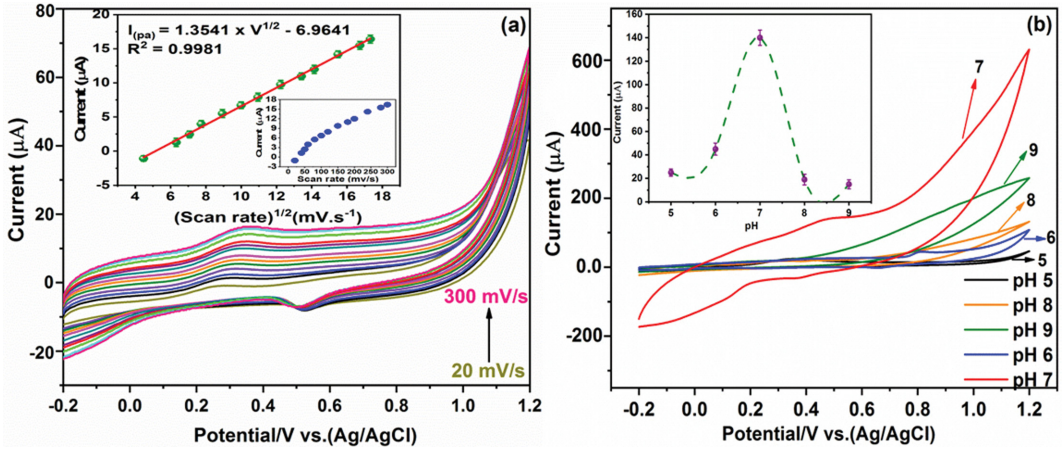

Fig. 5. (a) CV curves of Au-MoS_2/NiO/GCE in 0.1 M phosphate buffer (pH=7) containing 1 mM AA at different scan rates (20, 40, 50, 60, 80, 100, 120, 150, 180, 200, 240, 280, 300 mV s^{-1}) Inset: The plot of anodic peak currents against square root of scan rates, (b) CV curves of Au-MoS_2/NiO/GCE in 0.1 M buffer containing 1 mM AA at different pH (5, 6, 7,8, 9) at scan rate 50 mV s^{-1}. Inset: The plot of anodic peak currents against pH.

NiO/GCE for AA detection in 0.1 M phosphate buffer at scan rate 50 mV s^{-1} at different pHs. The effect of pH value was essential for modified electrode materials to display great pH stability pending detection. Fig. 5(b) inset illustrates the peak currents of pH solutions, and 0.1 M phosphate buffer pH 7 was chosen as electrolyte solution in this experiment with the highest current response. In similar studies, pH 7 was found suitable for ascorbic acid detection [3,46]. The peak current intensity boosted with the pH value changing from 5 to 7 and started to reduce from 7 to 9. The oxidation peak potential shift in the potential direction and the change in the current with the pH increase indicate the participation of protons during the oxidation of AA at the electrode surface [4]. It can be deduced that the oxidation of AA was performed by the mechanism given below on electrode and chemical reactions (Eqs. (2) and (3)) [4,47].

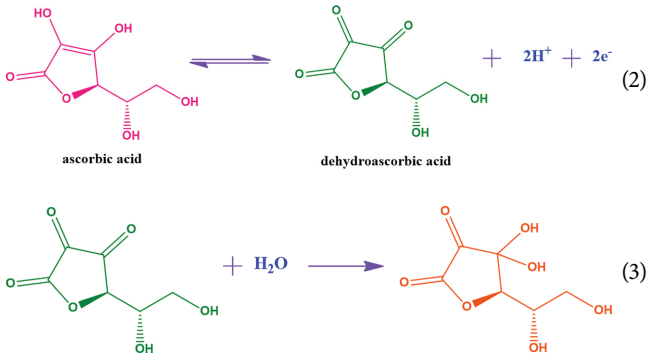

3. Analytical Performance of the Au-MoS_2/NiO Composite Modified GCE for Ascorbic Acid

Differential pulse voltammetry (DPV) is an important technique used in biosensors because of the main advantage of the low capacitive current, which can develop the sensitivity of the voltammetric procedure. So, the DPV technique has preferred the detection of AA. Fig. 6(a) shows the DPV current responses of the Au-MoS_2/NiO/GCE for AA at diverse concentrations (2-50 μM) in 0.1 M phosphate buffer (pH=7). With the increase in AA concentration, the peak potential of AA shifts to the right, indicating that protons have participated in the electrode reaction process of AA [48,49]. Fig. 6(b) demonstrates the corresponding calibration curve plotted from DPV response data. Fig. 6(b) inset depicts that the calibration curve of the Au-MoS_2/NiO/GCE sensor trails a hyperbolic trend at high AA concentration [50]. The first linear regression equation of current response vs. AA concentration was I (−mA)= −0.1579 $C_{(AA)}$ (μM)−3.689 (R^2=0.9946), corresponding sensitivity was 2.23 μA μM^{-1} cm^{-2} from 2 μM to 10 μM. The second linear regression equation of current response vs. AA concentration was I (−μA)=−0.084 $C_{(AA)}$ (μM)−5.758 (R^2=0.9560) is from 12 μM to 50 μM. The calibration graph shows a good linear relationship between the concentrations of the AA and oxidation currents from 2 to 50 μM with a linear correlation coefficient of R^2=0.9946.The detection limit was determined by considering the equation generally utilized for electrochemical sensors (LOD=3σ/S, where σ is the standard deviation of the ten parallel blank signals and S is the sensitivity of the calibration curve) [24,42,51]. The produced sensor demonstrated a linear detection range from 2 μM to 50 μM, with an LOD of 0.13 μM.

The analytical performance of the presented Au-MoS_2/NiO/GCE electrochemical sensor was also compared with the previous sensors based on AA determination in Table 1. In particular, compared to the AA sensors based on NiO and MoS_2 in Table 1 [11,18,52], the LOD value of this study was found to be quite low, which can be explained by synthesizing an excellent nanocomposite material, and the modification on GCE was created very well. This low detection limit is significant for detecting of low amounts of AA in some real samples [50]. According to Table 1, it can be seen that the modified electrode has superiorities in detection limit.

4. Studies of the Sensor Reproducibility, Stability and Interference

To investigate the reproducibility of the Au-MoS_2/NiO/GCE, the current responses of AA were studied using five electrodes under the same circumstances performed with comparing the DPV peak signals of 50 μM AA in 0.1 M phosphate buffer, pH 7.0 (Supplementary Material, Fig. S2). The result demonstrates that the rela-

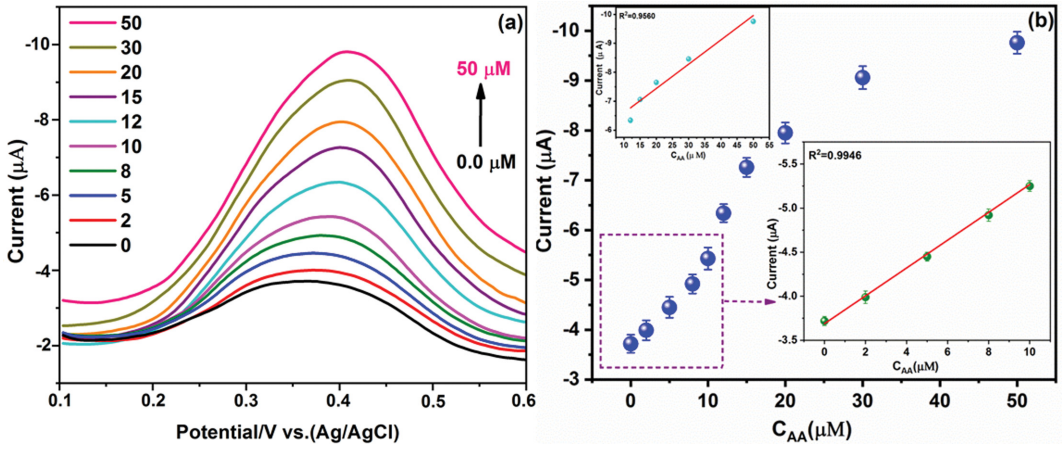

Fig. 6. (a) DPV curves of different concentrations (2-50 μM) of AA at the Au-MoS_2/NiO/GCE immersed in 0.1 M phosphate buffer (pH=7), (b) Calibration curve of DPV current at the Au-MoS_2/NiO/GCE as a function of AA concentration (Error bars represent triple evaluations of standard deviation calculation, n=3).

Table 1. Comparison of the Au-MoS_2/NiO/GCE with the different studies of AA detection

Materials	Technique	Linear ranges (μM)	LOD (μM)	References
MLN/Ag-GCE	Amperometry	30-1,000	15	[2]
Molybdophosphate/GCE	Amperometry	1-1,500	0.04	[5]
MoS_2/f-MWCNTs/ZnO	Amperometry	10-100	0.24	[11]
NiO/graphene modified graphite electrode	Amperometry	1-100	0.1	[18]
(Au/Ag/Pd)NPs/EPGrO/GCE	DPV	5-650	1.65	[45]
Nitrogen-doped reduced graphene oxide (N-rGO)	DPV	100-4,000	9.6	[51]
Hierarchical NiO/ITO	DPV	25-800	1.127	[52]
Mesoporous $CuCo_2O_4$/GCE	Amperometry	1-1,000	0.21	[53]
GQDs/IL-SPCE	DPV	25-400	6.64	[54]
GCE/Bi	DPV	10-70	0.697	[55]
Ti-C-Tx/GCE	DPV	100-1,000	4.64	[56]
Au-MoS_2/NiO/GCE	DPV	2-50	0.13	This study

Table 2. The recovery results of AA determination in Vitamin C tablet (n=3)

Sample	Added (μM)	Found (μM)	RSD (%)	Recovery (%)
Vitamin C tablet	0	-	-	-
	10	11.04	4.07	110.49
	20	16.57	3.77	82.87
	30	30.93	2.83	103.13
	40	39.77	2.44	99.44

tive standard deviation (RSD) of the Au-MoS_2/NiO/GCE sensor was estimated to be 2.9%. This demonstrates the impeccable reproducibility of the modified electrode. For the stability of the Au-MoS_2/NiO/GCE, Au-MoS_2/NiO/GCE was stored at 4 °C for four weeks. After one month of storage time, the sensor retained 82.7% of its primary response, representing good long-term stability (Supplementary Material, Fig. S3). The selectivity of the prepared Au-MoS_2/NiO/GCE was tested with the DPV response in the existence of various interfering reagents such as oxalic acid (OA), glucose (G), cysteine (C), and urea (U) (Supplementary Material, Fig. S4). Also, the selectivity of the Au-MoS_2/NiO/GCE toward AA was studied by calculating the peak current. The produced current responses were not significantly affected by the added interfering species. The above results show that Au-MoS2/NiO/GCE has remarkable selectivity, reproducibility, and superb stability for AA detection.

5. Application in Vitamin C Tablets as a Real Sample

The feasibility of the developed Au-MoS_2/NiO/GCE sensor for convenient application was appraised by detecting the AA concentration in Vitamin C tablets Vitamin C tablets (1,000 mg/tablet) utilized for the determination of AA were supplied from a local pharmacy. A vitamin C tablet was dissolved with 125 mL of deionized water. Subsequently, 20 μL of this solution was diluted 10 mL within 0.1 M phosphate buffer (pH=7.0), and AA was detected by the standard addition technique [12]. Recovery of AA was studied by the addition of five diverse concentrations of AA (10, 20, 30, and 40 μM) in Vitamin C tablet (Supplementary Material, Fig. S5). The recovery of the Vitamin C tablet was found in the range of 82.87-110.49% (Table 2). The obtained results showed that the application of the improved method was successfully implemented for the detection of AA in pharmaceutical and biological products.

CONCLUSION

Au-MoS_2/NiO/GCE indicates high electrocatalytic activity towards the oxidation of AA. This Au-MoS_2/NiO/GCE represents a much better electrocatalytic response for AA, with linearity from 2 to 50 μM and an LOD of 0.13 μM. It can be clearly concluded that the Au-MoS_2/NiO/GCE exhibited remarkable reproductivity and excellent stability, which could be related to the large surface area and high electrical conductivity of Au nanoparticles. In addition, the Au-MoS_2/NiO/GCE was successfully applied for the detection of AA in Vitamin C tablets. Also, the compositions of composites consisting of nanoparticles have major importance for developing the activity of nonenzymatic electrochemical sensors in the future.

ACKNOWLEDGEMENTS

We wish to thank the Scientific Research Projects Commission of Sakarya University (Project number: 2020-9-33-95) for the financial support of this study. M.O is grateful for Turkish Academy of Sciences (TUBA) for partial support.

CONFLICT OF INTEREST

We declare that we have no conflict of interest.

SUPPORTING INFORMATION

Additional information as noted in the text. This information is available via the Internet at http://www.springer.com/chemistry/journal/11814.

REFERENCES

1. K. Dhara and R. M. Debiprosad, *Anal. Biochem.*, **586**, 113415 (2019).
2. R. Zhao, Y. Wang, Z. Zhang, Y. Hasebe and D. Tao, *Anal. Sci.*, **35**, 733 (2019).
3. X. Zuo, H. Zhang and N. Li, *Sensors Actuators, B Chem.*, **161**, 1074 (2012).
4. Z. Bitew and M. Amare, *Org. Med. Chem.*, **8**, 1 (2019).
5. S. Liu, X. Jiang and M. Yang, *Microchim. Acta*, **186**, 1 (2019).
6. R. Bosma, J. Devasagayam, R. Eswar, I. F. Albuquerque and C. M. Collier, *Electrophoresis*, **41**, 1961(2020).
7. L. Han, J. Zhu, X. Fan, C. Zhang, K. Tu, J. Peng, J. Wang and L. Pan, *Sensors (Switzerland)*, **20**, 1 (2020).
8. J. Jia, M. Wu, S. Wang, X. Wang, Y. Hu, H. Chen, Y. Yu, C. Shen, H. Fu and Y. She, *Sensors Actuators, B Chem.*, **320**, 128256 (2020).
9. M. O. Gorbunova, V. V. Apyari, A. A. Baulina, M. S. Garshina, M. S. Kulyaginova, A. V. Shevchenko, A. A. Furletov, S. G. Dmitrienko and Y. A. Zolotov, *Talanta*, **219**, 121254 (2020).
10. Y. Hu, Y. He, Z. Peng and Y. Li, *Biosens. Bioelectron.*, **167**, 112490 (2020).
11. N. Murugan, T. H. V. Kumar, N. R. Devi and A. K. Sundramoorthy, *New J. Chem.*, **43**, 15105 (2019).
12. W. Argoubi, A. Rabti, N. Raouafi and S. B. Aoun, *RSC Adv.*, **9**, 37384 (2019).
13. T. H. V. Kumar, S. K. Yadav and A. K. Sundramoorthy, *J. Electrochem. Soc.*, **165**, B848 (2018).
14. G. Jeevanandham, R. Jerome, N. Murugan, M. Preethika, K. Vediappan and A. K. Sundramoorthy, *RSC Adv.*, **10**, 643 (2019).
15. D. Song, Y. Wang, X. Lu, Y. Gao, Y. Li and F. Gao, *Sensors Actuators, B Chem.*, **267**, 5 (2018).
16. X. Yang, Y. Tang, M. Wei, L. Chen, Q. Liu, P. Wang, Q. Wu, C. Wang and M. Zhang, *J. Electroanal. Chem.*, **841**, 36 (2019).
17. K. Annadurai, V. Sudha, G. Murugadoss and R. Thangamuthu, *J. Alloys Compd.*, **852**, 156911 (2021).
18. B. K. Swamy, K. Shiprath, G. Rakesh, K. V. Ratnam, H. Manjunatha, S. Janardan, K. C. B. Naidu, S. Ramesh, S. Babu and A. Ratnamala, *Biointerface Res. Appl. Chem.*, **10**, 5599 (2020).
19. N. R. Devi, M. Sasidharan and A. K. Sundramoorthy, *J. Electrochem. Soc.*, **165**, B3046 (2018).
20. Y. L. T. Ngo, L. T. Hoa, J. S. Chung and S. H. Hur, *J. Alloys Compd.*, **712**, 742 (2017).
21. H. Chen, H. Chen and R. Hong, *Catalysts*, **9**, 1 (2019).
22. H. Yu, J. Xu, Z. Liu, Y. Li and Z. Jin, *J. Mater. Sci.*, **53**, 15271 (2018).
23. K. Atacan, *J. Alloys Compd.*, **791**, 391 (2019).
24. A. Jirjees Dhulkefl, K. Atacan, S. Z. Bas and M. Ozmen, *Anal. Methods*, **12**, 499 (2020).
25. M. Carbone and P. Tagliatesta, *Materials (Basel)*, **13**, 1 (2020).
26. L. A. García-Cerda, K. M. Bernal-Ramos, S. M. Montemayor, M. A. Quevedo-López, R. Betancourt-Galindo and D. Bueno-Báques, *J. Nanomater.*, **2011**, 1 (2011).
27. S. Sagadevan and J. Podder, *Int. J. Nanoparticles*, **8**, 289 (2015).
28. S. Krishnamurthy, A. Esterle, N. C. Sharma and S. V. Sahi, *Nanoscale Res. Lett.*, **9**, 1 (2014).
29. X. Zhou, L. Xu, J. Lv, S. Yang, S. Zhu, X. Chen, X. Sun, B. Dong, X. Bai, G. Lu and H. Song, *Sensors Actuators, B Chem.*, **297**, 126729 (2019).
30. A. Rahdar, M. Aliahmad and Y. Azizi, *J. Nanostructures*, **5**, 145 (2015).
31. S. T. Fardood, A. Ramazani and S. Moradi, *Chem. J. Mold.*, **12**, 115 (2017).
32. B. I. Nandapure, S. B. Kondawar, A. M. Chaudhari and D. V. Jamkar, *Int. J. Curr. Eng. Sci. Res.*, **6**, 438 (2019).
33. P. Gogoi, B. J. Saikia and S. K. Dolui, *J. Appl. Polym. Sci.*, **132**, 1 (2015).
34. S. Samakchi, N. Chaibakhsh and Z. Moradi-Shoeili, *J. Photochem. Photobiol. A Chem.*, **367**, 420 (2018).
35. G. Zeng, W. Li, S. Ci, J. Jia and Z. Wen, *Sci. Rep.*, **6**, 1 (2016).
36. H. Y. Yue, H. J. Zhang, S. Huang, X. Gao, S. S. Song, Z. Wang, W. Q. Wang and E. H. Guan, *J. Mater. Sci. Mater. Electron.*, **30**, 5000 (2019).
37. W. Liu, C. Lu, X. Wang, K. Liang and B. K. Tay, *J. Mater. Chem. A*, **3**, 624 (2015).
38. G. Zhan, J. Zhang, Y. Wang, C. Yu, J. Wu, J. Cui, X. Shu, Y. Qin, H. Zheng, J. Sun, J. Yan, Y. Zhang, C. S. Tiwary and Y. Wu, *J. Colloid Interface Sci.*, **566**, 411 (2020).
39. Z. Li, S. Deng, R. Xu, L. Wei, X. Su and M. Wu, *Electrochim. Acta*, **252**, 200 (2017).
40. M. Nasrollahzadeh, N. Shafiei, M. Eslamipanah, P. Fakhri, B. Jaleh, Y. Orooji and R. S. Varma, *Clean Technol. Environ. Policy*, **22**, 1715 (2020).
41. E. S. Gomes, F. R. F. Leite, B. R. L. Ferraz, H. A. J. L. Mourão and A. R. Malagutti, *J. Pharm. Anal.*, **9**, 347 (2019).
42. N. Demir, K. Atacan, M. Ozmen and S. Z. Bas, *New J. Chem.*, **44**, 11759 (2020).
43. R. Sha and T. K. Bhattacharyya, *Electrochim. Act.*, **349**, 136370 (2020).
44. E. Mahmoudi, A. Hajian, M. Rezaei, A. Afkhami, A. Amine and H. Bagheri, *Microchem. J.*, **145**, 242 (2019).
45. A. A. Abdelwahab, A. M. Elseman, N. F. Alotaibi and A. M. Nassar, *Microchem. J.*, **156**, 104927 (2020).
46. Y. Li, W. Ye, Y. Cui, B. Li, Y. Yang and G. Qian, *J. Mol. Struct.*, **1209**, 127986 (2020).
47. C. S. Erdurak-Kiliç, B. Uslu, B. Dogan, U. Ozgen, S. A. Ozkan and M. Coskun, *J. Anal. Chem.*, **61**, 1113 (2006).
48. Y. Wei, Y. Liu, Z. Xu, S. Wang, B. Chen, D. Zhang and Y. Fang, *Int. J. Anal. Chem.*, **2020**, 1 (2020).
49. N. K. Bhajanthri, V. K. Arumugam, R. Chokkareddy and G. G. Redhi, *J. Mol. Liq.*, **222**, 370 (2016).
50. C. Kaçar and P. E. Erden, *Anal. Bioanal. Chem.*, **412**, 5315 (2020).
51. H. Zhang and S. Liu, *J. Alloys Compd.*, **842**, 155873 (2020).
52. M. Y. Emran, M. A. Shenashen, A. A. Abdelwahab, H. Khalifa, M. Mekawy, N. Akhtar, M. Abdelmottaleb and S. A. El-Safty, *J. Appl. Electrochem.*, **48**, 529 (2018).
53. X. Xiao, Z. Zhang, F. Nan, Y. Zhao, P. Wang, F. He and Y. Wang, *J. Alloys Compd.*, **852**, 157045 (2021).
54. K. Kunpatee, S. Traipop, O. Chailapakul and S. Chuanuwatanakul, *Sensors Actuators, B Chem.*, **314**,128059 (2020).
55. C. Van der Horst, B. Silwana, E. Gil, E. Iwuoha and V. Somerset, *Electroanalysis*, **32**, 1 (2020).
56. N. Murugan, R. Jerome, M. Preethika, A. Sundaramurthy and A. K. Sundramoorthy, *J. Mater. Sci. Technol.*, **72**, 122 (2021).

Supporting Information

Preparation of gold decorated MoS_2/NiO nanocomposite in the production of a new electrochemical sensor for ascorbic acid detection

Keziban Atacan*,,†, Nuray Güy**,***, and Mahmut Özacar**,***

*Sakarya University, Biomedical, Magnetic and Semiconductor Materials Application and Research Center (BIMAS-RC), 54187 Sakarya, Turkey

**Sakarya University, Biomaterials, Energy, Photocatalysis, Enzyme Technology, Nano & Advanced Materials, Additive Manufacturing, Environmental Applications and Sustainability Research & Development Group (BIOENAMS R & D Group), 54187 Sakarya, Turkey

***Sakarya University, Science & Arts Faculty, Department of Chemistry, 54187 Sakarya, Turkey

(*Received 26 October 2021 • Revised 4 December 2021 • Accepted 13 December 2021*)

Reagents and Apparatus

Ammonium molybdate tetrahydrate ($(NH_4)_6Mo_7O_{24}$, 99%), thiourea (CH_4N_2S, 99%), nickel(II) chloride hexahydrate ($NiCl_2{\cdot}6H_2O$, 97%), gold standard solution (1,000 ppm), sodium borohydride ($NaBH_4$, ≥96%) and ethanol (>99.2%) were obtained from Merck (Germany). NaH_2PO_4 and Na_2HPO_4 were provided from Sigma-Aldrich (USA). For the aqueous solutions, deionized water (Water Pro BT purification system, Labconco) was used.

All the prepared samples were confirmed by X-ray diffraction (XRD) pattern with PAN-alytical Empyrean diffractometer using Cu Kα irradiation (l=0.1542 nm) at 60 kV. Fourier transform infrared (FTIR) spectra of all samples were obtained from a Perkin Elmer FTIR Spectrometer (Spectrum Two) with the transmission mode. The morphological characterization of all samples were performed on the scanning electron microscope (SEM, ZEISS SİGMA 300). Electrochemical impedance spectroscopy (EIS) was acquired on a CHI 660C electrochemical workstation (CH Instruments, USA) in 0.1 M KCl containing $K_{3/4}Fe(CN)_6$ for all modified GCE with AC frequency range from 0.01 Hz to 1,000 Hz. All electrochemical measurements were carried out using an electrochemical workstation (CHI 660C model potentiostat,) connected to a computer with modified glassy carbon electrodes as the working electrode, an Ag/AgCl (1 M KCl) as reference electrode and a platinum (Pt) wire as counter electrode, respectively. All experiments were performed at room temperature.

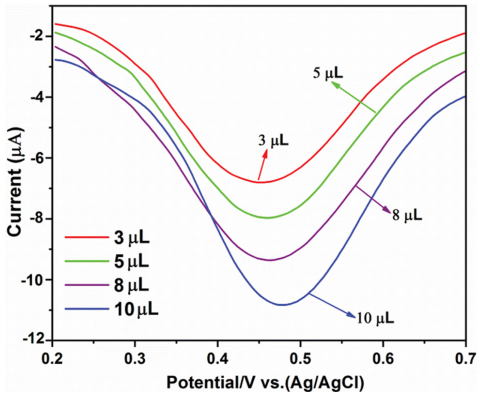

Fig. S1. DPVs of Au-MoS_2/NiO/GCE fabricated with various volumes (3, 5, 8 and 10 μL) of the composite for the detection of 50 μM AA in 0.1 M phosphate buffer (pH 7.0).

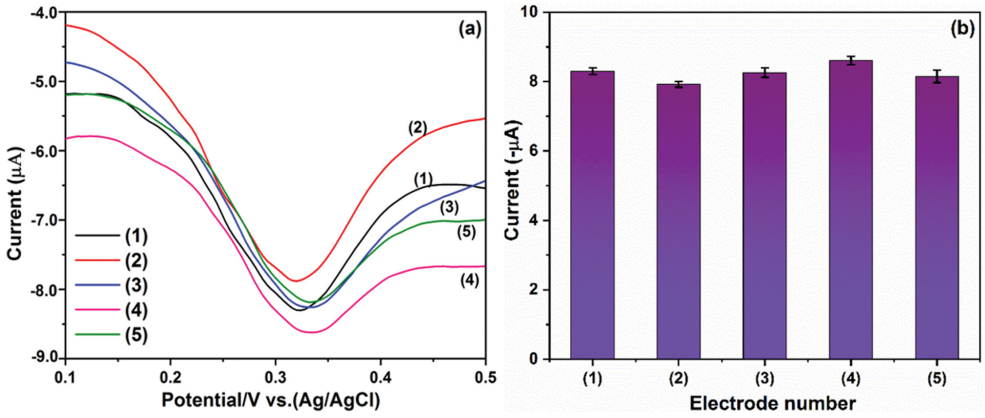

Fig. S2. (a) Reproducibility of five different electrodes by measuring the response to 50 μM AA in 0.1 M phosphate buffer (pH 7.0) by conducting the DPV technique (b) Column graph of DPV signals of AA recorded at Au-MoS_2/NiO/GCE at five different electrode prepared under the same conditions.

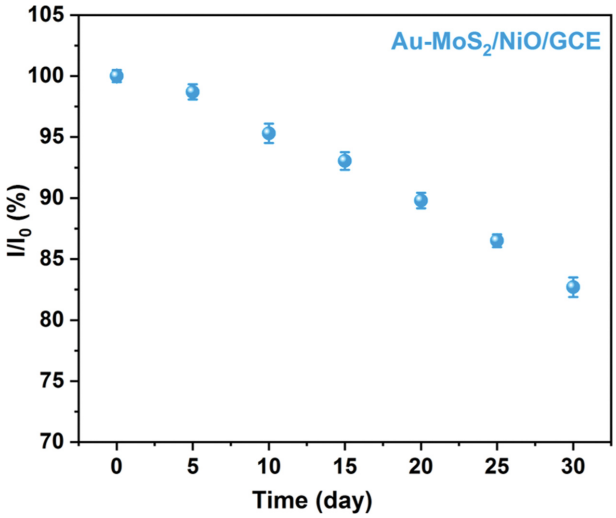

Fig. S3. Stability of Au-MoS_2/NiO/GCE at 4 °C for a period time of four weeks.

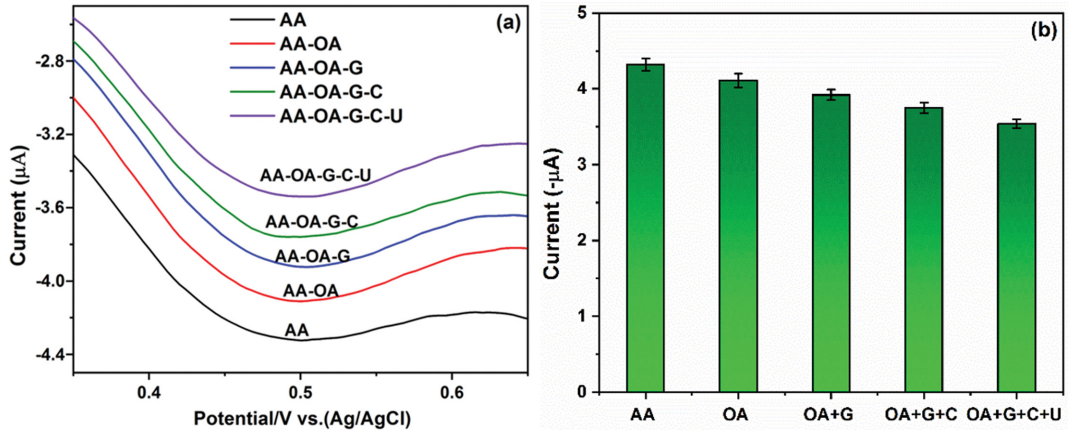

Fig. S4. (a) The interference studies with the DPV response in 0.1 M phosphate buffer (pH 7.0) (b) Column graph of DPV signals of recorded at Au-MoS_2/NiO/GCE in 0.1 M phosphate buffer (pH 7.0) containing 50 μM AA; the mixture of 50 μM AA and 100 μM OA; the mixture of 50 μM AA, 100 μM OA and 100 μM G; the mixture of 50 μM AA, 100 μM OA, 100 μM G and 100 μM C; the mixture of 50 μM AA, 100 μM OA, 100 μM G, 100 μM C and 100 μM U.

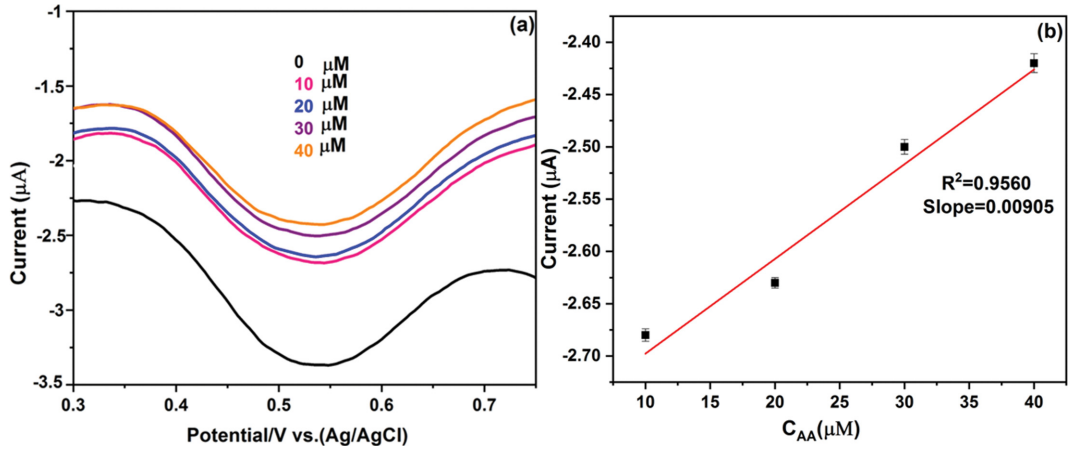

Fig. S5. (a) DPV responses of Au-MoS_2/NiO/GCE in diluted 20 μL of Vitamin C tablet within 0.1 M phosphate buffer (pH=7.0) by the addition of five diverse concentrations of AA (0, 10, 20, 30, and 40 μM) and (b) Determination of AA in Vitamin C tablet by using the equation derived from the calibration curve.